PROCEEDINGS OF SCIENCE

Updated results on neutrino Non-Standard Interactions with KM3NeT/ORCA6

Alfonso Lazo Pedrajas on behalf of the KM3NeT Collaboration[a,*]

[a] *IFIC - Instituto de Física Corpuscular (CSIC - Universitat de València), c/Catedrático José Beltrán, 2, 46980 Paterna, Valencia, Spain*

E-mail: Alfonso.Lazo@ific.uv.es

KM3NeT/ORCA is an underwater neutrino telescope currently under construction in the Mediterranean Sea, with the goal of measuring atmospheric neutrino oscillation parameters and determining the neutrino mass ordering. KM3NeT/ORCA can additionally provide constraints on physics beyond the Standard Model which could appear through strong matter effects, such as the neutrino Non-Standard Interactions (NSIs). This work reports on the results of the NSIs search with the final dataset of ORCA6, the first configuration of ORCA with six detection units, which uses 433 kton-years of exposure and improved calibration, reconstruction and selection methods compared to previous works. The obtained bounds at 90% CL, $|\varepsilon_{\mu\tau}| \leq 5.5 \cdot 10^{-3}$, $|\varepsilon_{e\tau}| \leq 7.8 \cdot 10^{-2}$, $|\varepsilon_{e\mu}| \leq 5.8 \cdot 10^{-2}$ and $-0.015 \leq \varepsilon_{\tau\tau} - \varepsilon_{\mu\mu} \leq 0.016$, are comparable to the current most stringent limits on any NSIs parameter.

38th International Cosmic Ray Conference (ICRC2023)
26 July - 3 August, 2023
Nagoya, Japan

*Speaker

PoS(ICRC2023)998

1. Introduction

1.1 Neutrino Non-Standard Interactions

The Neutrino Non-Standard Interactions (NSIs) appear naturally in several extensions of the Standard Model (SM) proposing mechanisms for the origin of neutrino masses. NSIs are incorporated through effective four-fermion interactions which lead to both charged-current (CC) and neutral-current (NC) interactions. NC NSIs affect the coherent forward scattering of neutrinos on fermions in matter, ultimately leading to modifications of neutrino oscillation probabilities in matter potentials. In the ultrarelativistic limit, neutrino propagation in matter is governed by the effective Hamiltonian $\mathcal{H}_{\text{eff}} = \mathcal{H}_{\text{vac}} + \mathcal{H}_{\text{SI}} + \mathcal{H}_{\text{NSIs}}$ given by [2]

$$\mathcal{H}_{\text{eff}} = \frac{1}{2E}\mathcal{U}\begin{bmatrix} 0 & 0 & 0 \\ 0 & \Delta m^2_{21} & 0 \\ 0 & 0 & \Delta m^2_{31} \end{bmatrix}\mathcal{U}^{+} + A(x)\begin{bmatrix} 1+\varepsilon_{ee} & \varepsilon_{e\mu} & \varepsilon_{e\tau} \\ \varepsilon^*_{e\mu} & \varepsilon_{\mu\mu} & \varepsilon_{\mu\tau} \\ \varepsilon^*_{e\tau} & \varepsilon^*_{\mu\tau} & \varepsilon_{\tau\tau} \end{bmatrix}, \tag{1}$$

where $A(x) = \sqrt{2}G_F n_e(x)$ is the standard matter potential for the electron number density at a given point, and $\mathcal{U}$ is the three-flavour PMNS matrix. The NSIs strength is therefore measured relative to the standard electroweak interaction, and is parameterised by six independent parameters: the complex off-diagonal terms induce flavour-changing (FC) neutral current interactions ($\nu_\alpha + f \rightarrow \nu_\beta + f$), whereas the real diagonal parameters cause non-universal couplings of the different neutrino flavours to fermions.

Neutrino propagation in matter is sensitive to the vector part of the NC-NSIs lagrangian, and to the incoherent sum of the scattering amplitudes of neutrinos on the three types of fermions found in matter [2]. For this reason, NSIs are customarily parameterised as

$$\varepsilon_{\alpha\beta} = \varepsilon^{eV}_{\alpha\beta} + \frac{N_u}{N_e}\varepsilon^{uV}_{\alpha\beta} + \frac{N_d}{N_e}\varepsilon^{dV}_{\alpha\beta}, \tag{2}$$

where the fractions denote the relative abundance of electrons, u- and d-quarks inside neutral Earth matter. In the following, only the NSIs coupling to the d quark is considered, since other choices can be derived by a simple rescaling given by the relative abundance of the other fermions.

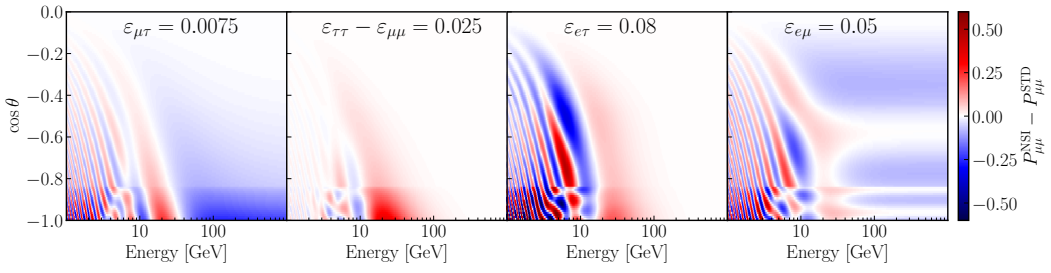

Figure 1: Difference in muon neutrino survival probability between the standard interaction case (STD) and four different non-zero NSIs hypothesis. Oscillation probabilities are computed numerically with the OscProb package [3].

Figure 1 presents the change induced by non-zero NSIs parameters (one at a time) to the muon neutrino survival probabilities. These are weighted according to the atmospheric flux composition and cross section ratio of $\nu_\mu/\bar{\nu}_\mu \sim 2$, with oscillation parameters fixed at the NuFit 5.0 values [4]. Given ORCA's current instrumented volume, NSIs effects are mostly accessible through modifications in the position and amplitude of the oscillation valley between 10 and 40 GeV. For $\varepsilon_{\mu\tau}$ and $\varepsilon_{e\mu}$, there are additional signatures at high energies (above 50 GeV) which are also observable with the current detector configuration.

1.2 The KM3NeT/ORCA detector

KM3NeT/ORCA is a water Cherenkov detector currently under construction in the Mediterranean Sea, 40 km offshore Toulon at a depth of around 2450 m [1]. Its main goal is the determination of the neutrino mass ordering (NMO) by studying the oscillations of few-GeV atmospheric neutrinos produced by cosmic ray interactions in the atmosphere. Neutrino interactions near or inside the instrumented volume produce secondary charged particles, whose Cherenkov light yield is detected by a three-dimensional grid of Digital Optical Modules (DOMs), housing 31 photomultiplier tubes (PMTs) each, in order to reconstruct the parent neutrino energy and direction based on the deposited light. By inspecting from horizontal to vertical neutrino arrival directions, KM3NeT/ORCA can probe baselines ranging from $\sim 10^2$ km to $O(10^4$ km) traversing different Earth layers, while being sensitive to energies between 1-100 GeV.

The detector is undergoing a modular construction with a final foreseen configuration of 115 vertical Detection Units (DUs), each housing 18 DOMs uniformly spaced every 9 m. DUs are deployed at the seabed following a layout with 20 m of inter-DU spacing and around 200 m of vertical length. Benefiting from this dense instrumentation, ORCA will be able to probe the low-energy range of the atmospheric neutrino spectrum (1-10 GeV) with unprecedented statistics. Since January 2020, the first configuration with six DUs (ORCA6) uninterruptedly took data until November 2021, when it was expanded with more detection units.

2. Event sample and selection

The dataset used in this work covers 433 kton-years of exposure of ORCA6, which were selected according to strict quality criteria on the environmental conditions and stability of the data-taking. The event filtering starts with a directional cut to keep up-going reconstructed events, followed by trigger and reconstruction quality requirements, efficiently rejecting most of the pure-noise background. The next level of event filtering uses the output of a Boosted Decision Tree (BDT), which was trained on reconstruction algorithm features to discriminate between atmospheric muons and neutrino-induced signal. The BDT cut allows to keep the atmospheric muon contamination in the sample below 5%, while retaining 60% of the neutrino signal from the previous selection level. Finally, a second BDT output discriminates between track-like topologies (ν_μ CC and ν_τ with subsequent τ muonic decays) and shower-like ones (ν_e CC, ν NC and remaining τ decays). The final sample comprises 5828 observed events split into three classes: high purity tracks with negligible atmospheric muon contamination and estimated 95% ν_μ-CC purity, low purity tracks with 4% muon contamination and 90% ν_μ-CC purity, and a shower class with 46% of muon neutrinos.

While the three are approximately equally populated, the high purity track class enhances the ν_μ-disappearance signal and renders the dataset the most sensitive to $\varepsilon_{\mu\tau}$ and $\varepsilon_{\tau\tau} - \varepsilon_{\mu\mu}$, whereas the shower class opens the possibility to constrain the electron NSIs sector ($\varepsilon_{e\tau}$ and $\varepsilon_{e\mu}$).

3. Analysis method

The analyses in ORCA proceed by comparing our observation with Monte Carlo (MC) templates weighted according to the hypothesis being tested. We use a Maximum Likelihood Estimator (MLE) of the NSIs and nuisance parameters, which uses the Poisson likelihood ($\mathcal{L}$) of observing the data given our MC expectation, binned in reconstructed zenith angle (baseline) versus reconstructed energy. Confidence intervals of the parameters are constructed by scanning the negative Log-Likelihood Ratio ($-2\log(\mathcal{L}_{NSIs}/\mathcal{L}_{bf}) = -2\Delta\log\mathcal{L}$) of each point in the NSIs space, computed using $\mathcal{L}$ at fixed NSIs over the likelihood at the global best fit. Fifteen nuisance parameters are profiled over in the MLE of the parameters. They model a variety of systematic uncertainties of the atmospheric neutrino flux (composition, energy and directional dependence), detector-related uncertainties (water properties, light propagation), interaction cross-section uncertainties (NC, ν_τ and individual class normalisations) and background modelling. Table 1 presents a summary of the nuisance and oscillation parameters with their assumed prior uncertainties, when applicable. The nominal oscillation parameter values are taken from NuFit 5.0 [4].

	Nominal value	**Syst. unc.**
$\Delta m^2_{31} \cdot 10^{-3}$ [eV^2]	2.517 (NO) /−2.424 (IO)	free
$\Delta m^2_{21} \cdot 10^{-5}$ [eV^2]	7.42	fixed
θ_{23} [°]	49.2 (NO) / 49.3 (IO)	free
θ_{21} [°]	33.44	fixed
θ_{31} [°]	8.57 (NO) / 8.60 (IO)	fixed
High purity Normalisation	1.0	free
Overall Normalisation	1.0	free
Shower Normalisation	1.0	free
Atm. Muon Normalisation	1.0	free
HE Light Sim	1.0	±50%
Energy Scale	1.0	±9%
Flux energy slope	0.0	±0.3
Flux zenith slope	0.0	±2%
ν_τ Norm	1.0	±20%
ν NC normalisation	1.0	±20%
$\nu_\mu/\bar{\nu}_\mu$	0.0	±5%
$\nu_e/\bar{\nu}_e$	0.0	±7%
ν_μ/ν_e	0.0	±2%

Table 1: Summary of the systematic uncertainties considered in this study.

4. Results

The one-by-one best fit NSIs parameters and 90% CL allowed regions, extracted from the $-2\Delta\log\mathcal{L}$ scans to the data assuming Wilks' theorem [5], are presented in table 2. No significant deviation from the standard interaction hypothesis was found for any NSIs parameter, with p-values ranging from 0.23 to 0.90.

Hypothesis	**Best fit** $\lvert\varepsilon_{ij}\rvert,\ \delta_{ij}$	**p-value**	**Real-valued 90% CL limit**	**Complex 90% CL limit**
$\varepsilon_{\mu\tau}$	$0.001^{+0.003}_{-0.001},\ 0^{+360°}_{-0}$	0.66	$[-0.0047, 0.0052]$	$\leq 0.0055,\ \delta_{\mu\tau} \in [0°, 360°]$
$\varepsilon_{\tau\tau} - \varepsilon_{\mu\mu}$	0.00 ± 0.01	0.90	$[-0.015, 0.016]$	—
$\varepsilon_{e\tau}$	$0.04 \pm 0.03,\ 190 \pm 70°$	0.23	$[-0.077, 0.028]$	$\leq 0.078,\ \delta_{e\tau} \in [0°, 360°]$
$\varepsilon_{e\mu}$	$0.03 \pm 0.02,\ 140 \pm 70°$	0.25	$[-0.056, 0.043]$	$\leq 0.058,\ \delta_{e\mu} \in [0°, 360°]$

Table 2: Best fit results and 90% CL limits for the NSIs parameters from the fits to the data.

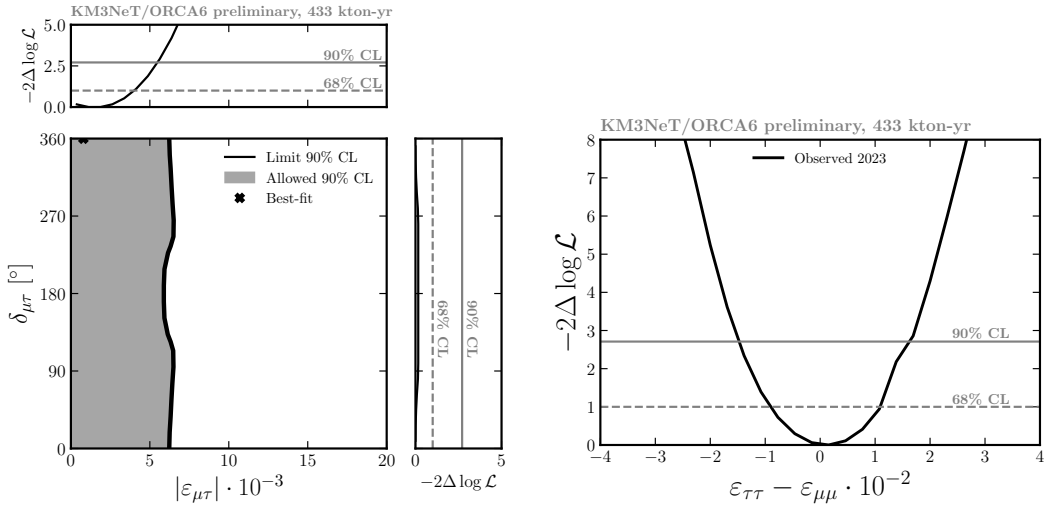

(a) $-2\Delta\log\mathcal{L}$ contour of $|\varepsilon_{\mu\tau}|$ vs $\delta_{\mu\tau}$.

(b) $-2\Delta\log\mathcal{L}$ scan of $\varepsilon_{\tau\tau} - \varepsilon_{\mu\mu}$.

Figure 2: Likelihood ratio contour at 90% CL of the complex parameter $\varepsilon_{\mu\tau}$ (2a) and profile of the real parameter $\varepsilon_{\tau\tau} - \varepsilon_{\mu\mu}$. In 2a, the top and side plots show the projections of $-2\Delta\log\mathcal{L}$ when the other variable is profiled over.

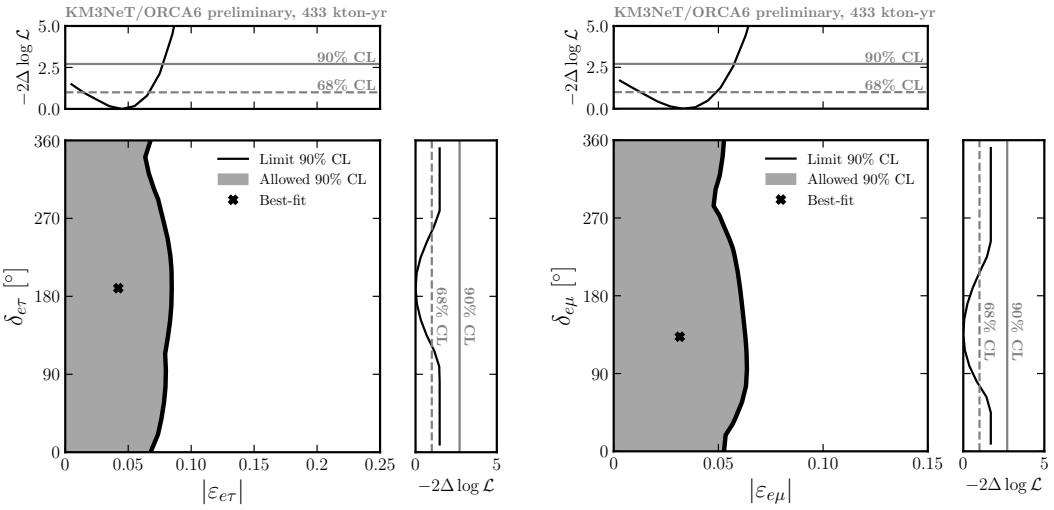

(a) $-2\Delta\log\mathcal{L}$ contour of $|\varepsilon_{e\tau}|$ vs $\delta_{e\tau}$ at 90% CL.

(b) $-2\Delta\log\mathcal{L}$ contour of $|\varepsilon_{e\mu}|$ vs $\delta_{e\mu}$ at 90% CL.

Figure 3: Likelihood ratio contour at 90% CL of the complex parameters $\varepsilon_{e\tau}$ (3a) and $\varepsilon_{e\mu}$ (3b). The top and side plots show the projections of $-2\Delta\log\mathcal{L}$ when the other variable is profiled over.

Figures 2a, 2b, 3a and 3b show the allowed regions obtained from this study. No sensitivity at 90% CL was observed for the complex phases of the flavour-violating NSIs coupling strengths, although somewhat stronger bounds are placed on $|\varepsilon_{e\tau}|$ and $|\varepsilon_{e\mu}|$ when their corresponding complex phases are restricted outside the range $[90°, 270°]$ and $[45°, 240°]$, respectively. Given the reduced sensitivity of ORCA6 to the NMO and θ_{23}-octant, $-2\Delta\log\mathcal{L}$ is profiled over the two assumed neutrino mass orderings and the two octants as starting points for the fits.

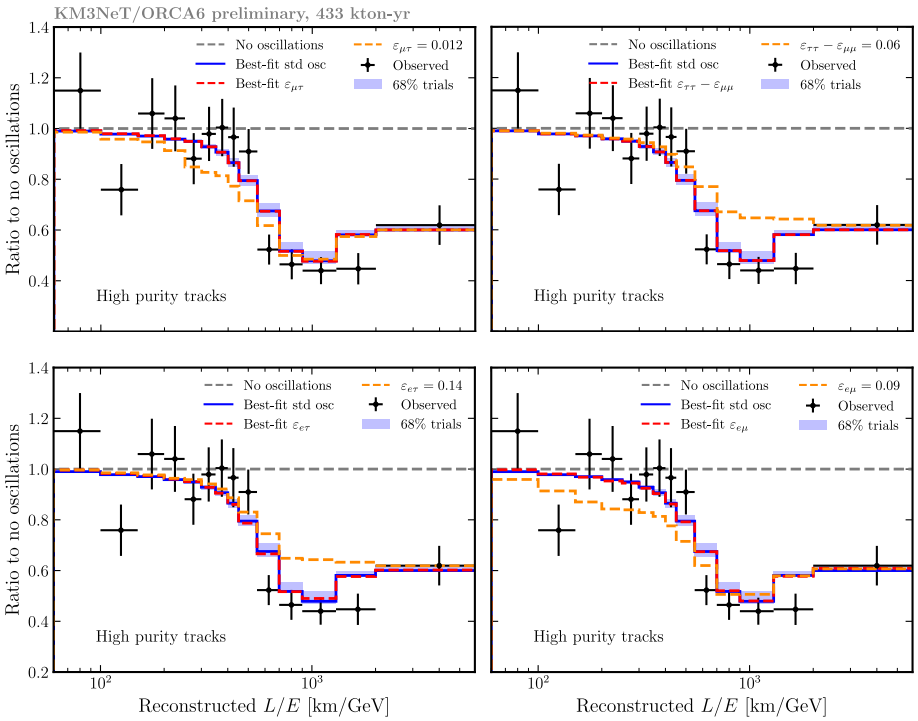

Figure 4: Ratio of events respect to the no oscillation hypothesis as a function of the baseline over reconstructed energy bin (L/E). The observed ratios are shown together with the prediction from the fits to five different hypothesis: the standard oscillation best fit (all), $\varepsilon_{\mu\tau}$ best fit, $\varepsilon_{\tau\tau} - \varepsilon_{\mu\mu}$ best fit, $\varepsilon_{e\tau}$ best fit and $\varepsilon_{e\mu}$ best fit. The 68% trials band is drawn by fitting the standard oscillation hypothesis to 1000 pseudo-experiments, generated from Poisson fluctuations of the data best-fit MC template under standard oscillations. Additionally, the yellow lines overlaid on every plot show the expectation from shifting each NSIs parameter to its 5σ limit, while keeping all systematic values at their best fit.

Figure 4 presents the number of observed and expected events as a function of L/E (baseline over reconstructed energy) for different oscillation best-fit scenarios, normalised to the expectation for the no-oscillation case. All distributions are shown only for the high purity track class, which is the most sensitive set to neutrino oscillations out of the three classes fit in the analysis. The oscillation valley between 300 and 2000 km/GeV is clearly visible in data and all expectations. For the four NSIs best fits, the resulting distributions follow closely the standard oscillation case, since no significant pull was observed on any coupling strength. For comparison, yellow dashed curves show the expectation from shifting each NSIs parameter alone at its 5σ threshold, while keeping all systematic values at their corresponding best fit. The effects observed in these shifts are fully compatible with the oscillation probabilities computed numerically in figure 1.

In the following, the impact of each systematic on the individual NSIs coupling strengths is studied, in correlation to the rest of the systematics set. The approach followed consists in shifting the value of one systematic at a time $\pm 1\sigma$ away from its best fit value for the given NSIs parameter, fix it and fit the remaining systematics together with the parameter of interest (PoI, the NSIs parameters in our case). The impact of the systematic shift is reflected as a deviation in the

PoI from its best fit to the data, divided by the 1σ uncertainty obtained in the real-valued profile of the PoI. Only deviations in the absolute value of the PoI are considered, since the NMO profiling during the fits can lead to sign flips in the PoI. This procedure yields the bar plots shown in figures 5a, 5b, 5c and 5d. On top of the bars, the black dots show the pulls exhibited by the systematics in the NSIs fits, where all nuisance parameters were free to vary. For this, the central values of the oscillation parameters were those of table 1 for NO , since $\Delta m^2_{31} > 0$ was preferred for the four NSIs fits. As can be seen, all constrained nuisance parameters were found well within their expectation.

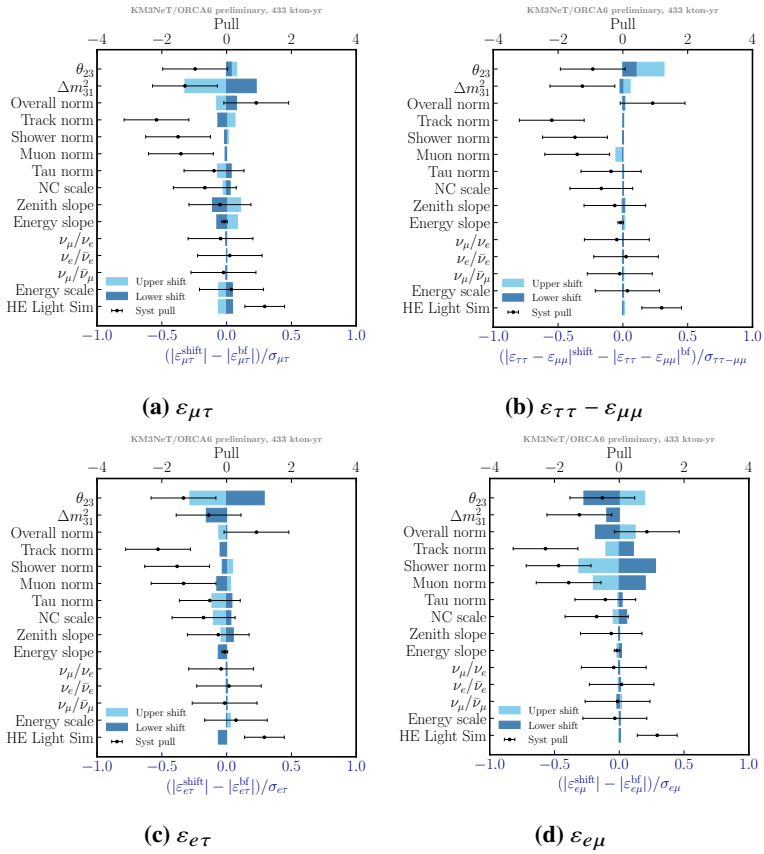

(a) $\varepsilon_{\mu\tau}$ **(b)** $\varepsilon_{\tau\tau} - \varepsilon_{\mu\mu}$

(c) $\varepsilon_{e\tau}$ **(d)** $\varepsilon_{e\mu}$

Figure 5: Systematics shift plot for the one-by-one NSIs coupling strengths. The light and dark blue bars reflect the shift exerted on the PoI by the upper and lower shift of the systematic, respectively. The bars are to be read with the lower blue axis. The overlaid black dots are the pulls experienced by the systematics in the NSIs fit, $(\text{syst}^{\text{bf}} - \text{syst}^{\text{nom}})/\sigma^{\text{syst}}$, being syst^{nom} the nominal values from table 1, and σ^{syst} is the prior width for constrained systematics, or the post fit 1σ uncertainty for unconstrained ones. The pulls are to be read with the upper black axis. The horizontal error bars on the pulls are the ratio of the post fit uncertainty to the prior width. For unconstrained parameters which do not have priors, the error bars are set to one unit.

Figure 5 then shows that the oscillation parameters Δm^2_{31} and θ_{23} have the biggest impact among all nuisance parameters, followed by the class normalisations, based on their shifts induced on the PoI. In particular, Δm^2_{31} appears as the most important systematic for $\varepsilon_{\mu\tau}$, due to both parameters being able to shift the position of the oscillation valley, whereas θ_{23} is the one for the remaining NSIs parameters, driven by the similar effects produced on the oscillation valley amplitude by varying the value of θ_{23} and $\varepsilon_{\tau\tau} - \varepsilon_{\mu\mu}$ or $\varepsilon_{e\tau}$. Finally, $\varepsilon_{e\mu}$ is most impacted by the shower class normalisation.

5. Summary and conclusions

This work reports on the results from the NSIs search with 433 kton-year of ORCA6. No significant deviation from standard interactions was found by measuring atmospheric neutrino oscillations with a sample of 5828 events, split into high purity tracks, low purity tracks and showers. The analysis has constrained NSIs coupling strengths at the 90% CL, assuming couplings to down quarks, to be $|\varepsilon_{\mu\tau}| \leq 5.5 \cdot 10^{-3}$, $|\varepsilon_{e\tau}| \leq 7.8 \cdot 10^{-2}$, $|\varepsilon_{e\mu}| \leq 5.8 \cdot 10^{-2}$ and $-0.015 \leq \varepsilon_{\tau\tau} - \varepsilon_{\mu\mu} \leq 0.016$. The resulting bounds are similar to the most stringent ones reported up to date, which are shown for real-valued NSIs parameters in figure 6, and still offer room for improvement in the near future, coming mainly from the extensions of ORCA's instrumented volume with more detection units.

Finally, the authors want to acknowledge the financial support from Generalitat Valenciana and the European Social Fund through the ACIF/2021/233 grant, and the support from Ministerio de Ciencia e Innovación (MCINN) through the programme PID2021-124591NB-C41.

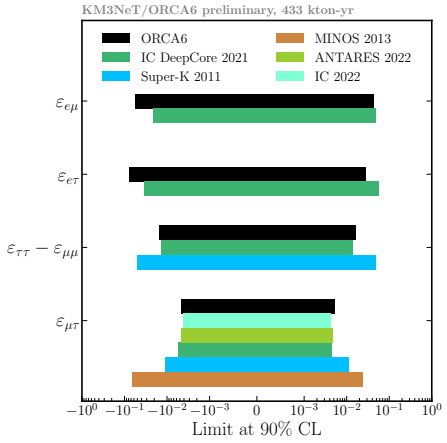

Figure 6: Comparison of the 90% CL limits reported in this work and DeepCore [6], IceCube [7], Super-K [8], ANTARES [9] and MINOS [10]. DeepCore and MINOS results were rescaled to match the down-quark coupling used by the other experiments, using the factor deduced from [6].

References

[1] KM3NeT Collaboration. DOI: 10.1088/0954-3899/43/8/084001.

[2] A. Chatterjee et al. DOI: https://doi.org/10.1103/PhysRevD.93.093017.

[3] J. Coelho et al. joaoabcoelho/OscProb: v1.6.1 (v.1.6.1). Zenodo. https://doi.org/10.5281/zenodo.8074017.

[4] I. Esteban et al. DOI: https://doi.org/10.1007/JHEP09(2020)178.

[5] S. Wilks. DOI: 10.1214/aoms/1177732360.

[6] IceCube Collaboration. DOI: https://doi.org/10.1103/PhysRevD.104.072006.

[7] IceCube Collaboration. DOI: https://doi.org/10.1103/PhysRevLett.129.011804.

[8] Super-Kamiokande Collaboration. DOI: https://doi.org/10.1103/PhysRevD.84.113008.

[9] ANTARES collaboration. DOI: https://doi.org/10.1007/JHEP07(2022)048.

[10] MINOS collaboration. DOI: https://doi.org/10.1103/PhysRevD.88.072011.

Full Authors List: The KM3NeT Collaboration

S. Aiello[a], A. Albert[b,bd], S. Alves Garre[c], Z. Aly[d], A. Ambrosone[f,e], F. Ameli[g], M. Andre[h], E. Androutsou[i], M. Anguita[j], L. Aphecetche[k], M. Ardid[l], S. Ardid[l], H. Atmani[m], J. Aublin[n], L. Bailly-Salins[o], Z. Bardačová[q,p], B. Baret[n], A. Bariego-Quintana[c], S. Basegmez du Pree[r], Y. Becherini[n], M. Bendahman[m,n], F. Benfenati[t,s], M. Benhassi[u,e], D. M. Benoit[v], E. Berbee[r], V. Bertin[d], S. Biagi[w], M. Boettcher[x], D. Bonanno[w], J. Boumaaza[m], M. Bouta[y], M. Bouwhuis[r], C. Bozza[z,e], R. M. Bozza[f,e], H.Brânzaş[aa], F. Bretaudeau[k], R. Bruijn[ab,r], J. Brunner[d], R. Bruno[a], E. Buis[ac,r], R. Buompane[u,e], J. Busto[d], B. Caiffi[ad], D. Calvo[c], S. Campion[g,ae], A. Capone[g,ae], F. Carenini[t,s], V. Carretero[c], T. Cartraud[n], P. Castaldi[af,s], V. Cecchini[c], S. Celli[g,ae], L. Cerisy[d], M. Chabab[ag], M. Chadolias[ah], A. Chen[ai], S. Cherubini[aj,w], T. Chiarusi[s], M. Circella[ak], R. Cocimano[w], J. A. B. Coelho[n], A. Coleiro[n], R. Coniglione[w] P. Coyle[d], A. Creusot[n], A. Cruz[al], G. Cuttone[w], R. Dallier[k], Y. Darras[ah], A. De Benedittis[e], B. De Martino[d], V. Decoene[k], R. Del Burgo[e], U. M. Di Cerbo[e], L. S. Di Mauro[w], I. Di Palma[g,ae], A. F. Díaz[j], C. Diaz[j], D. Diego-Tortosa[w], C. Distefano[w], A. Domi[ah], C. Donzaud[n], D. Dornic[d], M. Dörr[am], E. Drakopoulou[i], D. Drouhin[b,bd], R. Dvornický[q], T. Eberl[ah], E. Eckerová[q,p], A. Eddymaoui[m], T. van Eeden[r], M. Eff[n], D. van Eijk[r], I. El Bojaddaini[y], S. El Hedri[n], A. Enzenhöfer[d], G. Ferrara[w], M. D. Filipović[an], F. Filippini[t,s], D. Franciotti[w], L. A. Fusco[z,e], J. Gabriel[ao], S. Gagliardini[g], T. Gal[ah], J. García Méndez[l], A. Garcia Soto[c], C. Gatius Oliver[r], N. Geißelbrecht[ah], H. Ghaddari[y], L. Gialanella[e,u], B. K. Gibson[v], E. Giorgio[w], I. Goos[n], D. Goupilliere[o], S. R. Gozzini[c], R. Gracia[ah], K. Graf[ah], C. Guidi[ap,ad], B. Guillon[o], M. Gutiérrez[aq], H. van Haren[ar], A. Heijboer[r], A. Hekalo[am], L. Hennig[ah], J. J. Hernández-Rey[c], F. Huang[d], W. Idrissi Ibnsalih[e], G. Illuminati[s], C. W. James[al], M. de Jong[as,r], P. de Jong[ab,r], B. J. Jung[r], P. Kalaczyński[at,be], O. Kalekin[ah], U. F. Katz[ah], N. R. Khan Chowdhury[c], A. Khatun[q], G. Kistauri[av,au], C. Kopper[ah], A. Kouchner[aw,n], V. Kulikovskiy[ad], R. Kvatadze[av], M. Labalme[o], R. Lahmann[ah], G. Larosa[w], C. Lastoria[d], A. Lazo[c], S. Le Stum[d], G. Lehaut[o], E. Leonora[a], N. Lessing[c], G. Levi[t,s], M. Lindsey Clark[n], F. Longhitano[a], J. Majumdar[r], L. Malerba[ad], F. Mamedov[p], J. Mańczak[c], A. Manfreda[e], M. Marconi[ap,ad], A. Margiotta[t,s], A. Marinelli[e,f], C. Markou[i], L. Martin[k], J. A. Martínez-Mora[l], F. Marzaioli[u,e], M. Mastrodicasa[ae,g], S. Mastroianni[e], S. Miccichè[w], G. Miele[f,e], P. Migliozzi[e], E. Migneco[w], M. L. Mitsou[e], C. M. Mollo[e], L. Morales-Gallegos[u,e], C. Morley-Wong[al], A. Moussa[y], I. Mozun Mateo[ay,ax], R. Muller[r], M. R. Musone[e,u], M. Musumeci[w], L. Nauta[r], S. Navas[aq], A. Nayerhoda[ak], C. A. Nicolau[g], B. Nkosi[ai], B. Ó Fearraigh[ab,r], V. Oliviero[f,e], A. Orlando[w], E. Oukacha[n], D. Paesani[w], J. Palacios González[c], G. Papalashvili[au], V. Parisi[ap,ad], E.J. Pastor Gomez[c], A. M. Păun[aa], G. E. Păvălaş[aa], S. Peña Martínez[n], M. Perrin-Terrin[d], J. Perronnel[o], V. Pestel[ay], R. Pestes[n], P. Piattelli[w], C. Poirè[z,e], V. Popa[aa], T. Pradier[b], S. Pulvirenti[w], G. Quéméner[o], C. Quiroz[l], U. Rahaman[c], N. Randazzo[a], R. Randriatoamanana[k], S. Razzaque[az], I. C. Rea[e], D. Real[c], S. Reck[ah], G. Riccobene[w], J. Robinson[x], A. Romanov[ap,ad], A. Šaina[c], F. Salesa Greus[c], D. F. E. Samtleben[as,r], A. Sánchez Losa[c,ak], S. Sanfilippo[w], M. Sanguineti[ap,ad], C. Santonastaso[ba,e], D. Santonocito[w], P. Sapienza[w], J. Schnabel[ah], J. Schumann[ah], H. M. Schutte[x], J. Seneca[r], N. Sennan[y], B. Setter[ah], I. Sgura[ak], R. Shanidze[au], Y. Shitov[p], F. Šimkovic[q], A. Simonelli[e], A. Sinopoulou[a], M.V. Smirnov[ah], B. Spisso[e], M. Spurio[t,s], D. Stavropoulos[i], I. Štekl[p], M. Taiuti[ap,ad], Y. Tayalati[m], H. Tedjditi[ad], H. Thiersen[x], I. Tosta e Melo[a,aj], B. Trocmé[n], V. Tsourapis[i], E. Tzamariudaki[i], A. Vacheret[o], V. Valsecchi[w], V. Van Elewyck[aw,n], G. Vannoye[d], G. Vasileiadis[bb], F. Vazquez de Sola[r], C. Verilhac[n], A. Veutro[g,ae], S. Viola[w], D. Vivolo[u,e], J. Wilms[bc], E. de Wolf[ab,r], H. Yepes-Ramirez[l], G. Zarpapis[i], S. Zavatarelli[ad], A. Zegarelli[g,ae], D. Zito[w], J. D. Zornoza[c], J. Zúñiga[c], and N. Zywucka[x].

[a] INFN, Sezione di Catania, Via Santa Sofia 64, Catania, 95123 Italy
[b] Université de Strasbourg, CNRS, IPHC UMR 7178, F-67000 Strasbourg, France
[c] IFIC - Instituto de Física Corpuscular (CSIC - Universitat de València), c/Catedrático José Beltrán, 2, 46980 Paterna, Valencia, Spain
[d] Aix Marseille Univ, CNRS/IN2P3, CPPM, Marseille, France
[e] INFN, Sezione di Napoli, Complesso Universitario di Monte S. Angelo, Via Cintia ed. G, Napoli, 80126 Italy
[f] Università di Napoli "Federico II", Dip. Scienze Fisiche "E. Pancini", Complesso Universitario di Monte S. Angelo, Via Cintia ed. G, Napoli, 80126 Italy
[g] INFN, Sezione di Roma, Piazzale Aldo Moro 2, Roma, 00185 Italy
[h] Universitat Politècnica de Catalunya, Laboratori d'Aplicacions Bioacústiques, Centre Tecnològic de Vilanova i la Geltrú, Avda. Rambla Exposició, s/n, Vilanova i la Geltrú, 08800 Spain
[i] NCSR Demokritos, Institute of Nuclear and Particle Physics, Ag. Paraskevi Attikis, Athens, 15310 Greece
[j] University of Granada, Dept. of Computer Architecture and Technology/CITIC, 18071 Granada, Spain
[k] Subatech, IMT Atlantique, IN2P3-CNRS, Université de Nantes, 4 rue Alfred Kastler - La Chantrerie, Nantes, BP 20722 44307 France
[l] Universitat Politècnica de València, Instituto de Investigación para la Gestión Integrada de las Zonas Costeras, C/ Paranimf, 1, Gandia, 46730 Spain
[m] University Mohammed V in Rabat, Faculty of Sciences, 4 av. Ibn Battouta, B.P. 1014, R.P. 10000 Rabat, Morocco
[n] Université Paris Cité, CNRS, Astroparticule et Cosmologie, F-75013 Paris, France
[o] LPC CAEN, Normandie Univ, ENSICAEN, UNICAEN, CNRS/IN2P3, 6 boulevard Maréchal Juin, Caen, 14050 France
[p] Czech Technical University in Prague, Institute of Experimental and Applied Physics, Husova 240/5, Prague, 110 00 Czech Republic
[q] Comenius University in Bratislava, Department of Nuclear Physics and Biophysics, Mlynska dolina F1, Bratislava, 842 48 Slovak Republic
[r] Nikhef, National Institute for Subatomic Physics, PO Box 41882, Amsterdam, 1009 DB Netherlands
[s] INFN, Sezione di Bologna, v.le C. Berti-Pichat, 6/2, Bologna, 40127 Italy
[t] Università di Bologna, Dipartimento di Fisica e Astronomia, v.le C. Berti-Pichat, 6/2, Bologna, 40127 Italy
[u] Università degli Studi della Campania "Luigi Vanvitelli", Dipartimento di Matematica e Fisica, viale Lincoln 5, Caserta, 81100 Italy
[v] E. A. Milne Centre for Astrophysics, University of Hull, Hull, HU6 7RX, United Kingdom

[w] INFN, Laboratori Nazionali del Sud, Via S. Sofia 62, Catania, 95123 Italy
[x] North-West University, Centre for Space Research, Private Bag X6001, Potchefstroom, 2520 South Africa
[y] University Mohammed I, Faculty of Sciences, BV Mohammed VI, B.P. 717, R.P. 60000 Oujda, Morocco
[z] Università di Salerno e INFN Gruppo Collegato di Salerno, Dipartimento di Fisica, Via Giovanni Paolo II 132, Fisciano, 84084 Italy
[aa] ISS, Atomistilor 409, Măgurele, RO-077125 Romania
[ab] University of Amsterdam, Institute of Physics/IHEF, PO Box 94216, Amsterdam, 1090 GE Netherlands
[ac] TNO, Technical Sciences, PO Box 155, Delft, 2600 AD Netherlands
[ad] INFN, Sezione di Genova, Via Dodecaneso 33, Genova, 16146 Italy
[ae] Università La Sapienza, Dipartimento di Fisica, Piazzale Aldo Moro 2, Roma, 00185 Italy
[af] Università di Bologna, Dipartimento di Ingegneria dell'Energia Elettrica e dell'Informazione "Guglielmo Marconi", Via dell'Università 50, Cesena, 47521 Italia
[ag] Cadi Ayyad University, Physics Department, Faculty of Science Semlalia, Av. My Abdellah, P.O.B. 2390, Marrakech, 40000 Morocco
[ah] Friedrich-Alexander-Universität Erlangen-Nürnberg (FAU), Erlangen Centre for Astroparticle Physics, Nikolaus-Fiebiger-Straße 2, 91058 Erlangen, Germany
[ai] University of the Witwatersrand, School of Physics, Private Bag 3, Johannesburg, Wits 2050 South Africa
[aj] Università di Catania, Dipartimento di Fisica e Astronomia "Ettore Majorana", Via Santa Sofia 64, Catania, 95123 Italy
[ak] INFN, Sezione di Bari, via Orabona, 4, Bari, 70125 Italy
[al] International Centre for Radio Astronomy Research, Curtin University, Bentley, WA 6102, Australia
[am] University Würzburg, Emil-Fischer-Straße 31, Würzburg, 97074 Germany
[an] Western Sydney University, School of Computing, Engineering and Mathematics, Locked Bag 1797, Penrith, NSW 2751 Australia
[ao] IN2P3, LPC, Campus des Cézeaux 24, avenue des Landais BP 80026, Aubière Cedex, 63171 France
[ap] Università di Genova, Via Dodecaneso 33, Genova, 16146 Italy
[aq] University of Granada, Dpto. de Física Teórica y del Cosmos & C.A.F.P.E., 18071 Granada, Spain
[ar] NIOZ (Royal Netherlands Institute for Sea Research), PO Box 59, Den Burg, Texel, 1790 AB, the Netherlands
[as] Leiden University, Leiden Institute of Physics, PO Box 9504, Leiden, 2300 RA Netherlands
[at] National Centre for Nuclear Research, 02-093 Warsaw, Poland
[au] Tbilisi State University, Department of Physics, 3, Chavchavadze Ave., Tbilisi, 0179 Georgia
[av] The University of Georgia, Institute of Physics, Kostava str. 77, Tbilisi, 0171 Georgia
[aw] Institut Universitaire de France, 1 rue Descartes, Paris, 75005 France
[ax] IN2P3, 3, Rue Michel-Ange, Paris 16, 75794 France
[ay] LPC, Campus des Cézeaux 24, avenue des Landais BP 80026, Aubière Cedex, 63171 France
[az] University of Johannesburg, Department Physics, PO Box 524, Auckland Park, 2006 South Africa
[ba] Università degli Studi della Campania "Luigi Vanvitelli", CAPACITY, Laboratorio CIRCE - Dip. Di Matematica e Fisica - Viale Carlo III di Borbone 153, San Nicola La Strada, 81020 Italy
[bb] Laboratoire Univers et Particules de Montpellier, Place Eugène Bataillon - CC 72, Montpellier Cédex 05, 34095 France
[bc] Friedrich-Alexander-Universität Erlangen-Nürnberg (FAU), Remeis Sternwarte, Sternwartstraße 7, 96049 Bamberg, Germany
[bd] Université de Haute Alsace, rue des Frères Lumière, 68093 Mulhouse Cedex, France
[be] AstroCeNT, Nicolaus Copernicus Astronomical Center, Polish Academy of Sciences, Rektorska 4, Warsaw, 00-614 Poland

Acknowledgements

The authors acknowledge the financial support of the funding agencies: Agence Nationale de la Recherche (contract ANR-15-CE31-0020), Centre National de la Recherche Scientifique (CNRS), Commission Européenne (FEDER fund and Marie Curie Program), LabEx UnivEarthS (ANR-10-LABX-0023 and ANR-18-IDEX-0001), Paris Île-de-France Region, France; Shota Rustaveli National Science Foundation of Georgia (SRNSFG, FR-22-13708), Georgia; The General Secretariat of Research and Innovation (GSRI), Greece Istituto Nazionale di Fisica Nucleare (INFN), Ministero dell'Università e della Ricerca (MIUR), PRIN 2017 program (Grant NAT-NET 2017W4HA7S) Italy; Ministry of Higher Education, Scientific Research and Innovation, Morocco, and the Arab Fund for Economic and Social Development, Kuwait; Nederlandse organisatie voor Wetenschappelijk Onderzoek (NWO), the Netherlands; The National Science Centre, Poland (2021/41/N/ST2/01177); The grant "AstroCeNT: Particle Astrophysics Science and Technology Centre", carried out within the International Research Agendas programme of the Foundation for Polish Science financed by the European Union under the European Regional Development Fund; National Authority for Scientific Research (ANCS), Romania; Grants PID2021-124591NB-C41, -C42, -C43 funded by MCIN/AEI/ 10.13039/501100011033 and, as appropriate, by "ERDF A way of making Europe", by the "European Union" or by the "European Union NextGenerationEU/PRTR", Programa de Planes Complementarios I+D+I (refs. ASFAE/2022/023, ASFAE/2022/014), Programa Prometeo (PROMETEO/2020/019) and GenT (refs. CIDEGENT/2018/034, /2019/043, /2020/049. /2021/23) of the Generalitat Valenciana, Junta de Andalucía (ref. SOMM17/6104/UGR, P18-FR-5057), EU: MSC program (ref. 101025085), Programa María Zambrano (Spanish Ministry of Universities, funded by the European Union, NextGenerationEU), Spain; The European Union's Horizon 2020 Research and Innovation Programme (ChETEC-INFRA - Project no. 101008324).